Exploring CIE Lab Color Characteristics for Skin Lesion Images Detection: A Novel Image Analysis Methodology Incorporating Color-based Segmentation and Luminosity Analysis

Marwa Mawfaq M. Al-Hatab [1,*], Ahmed S. Ibrahim Al-Obaidi [2], Mohammad Abid Al-Hashim [3]

[1,2]Technical Engineering College /Northren Technical University, Mosul, Iraq

[3]Department of Computer Science /Collage of Computer Science and Mathematics / University of Mosul, Iraq

Emails: marwa.alhatab@ntu.edu.iq; ahmedsaeed@ntu.edu.iq; maqassim@uomosul.edu.iq

Abstract

Accurate classification of malignant and benign skin lesions is crucial in dermatology. In this novel research, we propose robust image analysis methodology for skin lesion classification that integrates color-based segmentation with luminosity analysis. Our approach is evaluated on a dataset of 400 skin images, with equal representation of malignant and benign samples. By computing mean color values for the Red Channel Color (RCC), Green Channel Color (GCC), and Blue Channel Color (BCC) in groups of 10 samples, we establish a classification range for precise diagnosis, this research introduces a novel dimension by harnessing the potential of the CIE Lab Color characteristics for skin lesion detection as the most reliable scale for distinguishing between benign and malignant samples. The smaller and more thought variety ranges saw in the glow examination improve difference and perceivability, consequently working with prevalent sore separation. By featuring the meaning of mean histograms for each variety channel, this complete exploration adds to propelling the area of dermatology and presents an imaginative methodology that holds guarantee for PC helped conclusion frameworks in skin malignant growth discovery.

Keywords: CIE lab color; Image segmentation; skin cancer detection.

1. Introduction

Skin disease is the most widely recognized sort of malignant growth around the world. One of the largest organs covering the human body is the skin [1], and early diagnosis is crucial to treatment. A common diagnostic approach is professional visual assessment [2], AI calculations have demonstrated to be significant apparatuses in supporting dermatologists in the early identification of skin malignant growth. [3]. The popular unsupervised learning algorithm known as K-means clustering has been successfully used to classify skin lesions. This approach exploits skin credits like tone, shape, and surface, which clinical specialists ordinarily consider while diagnosing skin conditions. [4].

The term non-melanoma skin disease relates to a bunch of malignancies that show a slow beginning inside the epidermal layers of the skin [5]. The epidermis, the skin's outermost layer, is where abnormal cells grow uncontrollably, which is the hallmark of skin cancer. This condition emerges because of the disappointment of DNA harm fix systems [6]. Cutaneous eruptions. Malignant neoplasms emerge because of the proliferation of skin cells brought on by these mutations. Skin disease incorporates a few essential characterizations, in particular basal cell carcinoma (BCC), squamous cell carcinoma (SCC), melanoma, and Merkel cell carcinoma (MCC) as illustrated in reference [7].

Basal cell carcinoma (BCC) has a low tendency to spread. On the other hand, squamous cell carcinoma (SCC) may have the potential to metastasize to lymph nodes in approximately 5% of cases. According to the 2020

Doi: https://doi.org/10.54216/FPA.150108
Received: August 12, 2023 Revised: December 10, 2023 Accepted: February 18, 2024

statistics compiled by the World Health Organization (WHO), the risk associated with skin cancer is evident, with over 1.5 million individuals diagnosed with skin cancer and an annual death toll of nearly 120,000 people [8]. In 2021, the American Cancer Society (ACS) projects 7,180 fatalities from melanoma out of a total of 106,110 cases [9].

Medullary cell carcinoma and breast cancer If left untreated, can affect the skin. 9 out of 10 cases of non-melanoma skin cancer, can be effectively treated. Sunlight exposure and the use of tanning beds are the primary factors contributing to the onset of skin cancer. When detected at an early stage, dermatologists have the capability to treat skin cancer without leaving noticeable scars and eliminate it. In some cases, medical professionals may identify abnormal growths before they develop into full-blown skin cancer or before they breach the skin [10].

In today's world, the application of machine learning to the detection and classification of skin cancer is becoming increasingly common. The viability of these calculations in diagnosing and supporting doctors in the location of skin sicknesses has been illustrated, bringing about an ideal effect on the arrangement of illness the board and patient consideration. An algorithm known as K-means clustering has demonstrated the capacity to produce favourable outcomes at this stage.

The ongoing review presents an interesting technique for distinguishing skin malignant growth that utilizes the K-implies calculation. The proposed method aims to improve diagnostic processes' efficacy and accuracy and classify skin lesions as benign or malignant. This is chiefly achieved by applying the K-implies grouping procedure and separating significant elements from pre-handled photographs of skin sores. The current investigation concerns the use of K-means clustering in the classification of skin diseases. This is achieved by means of the analysing of a set of picture data related to skin lesions. The results showed a high degree of accuracy in identifying and classifying skin disorders, which has significant promise for the prompt detection of both benign and malignant diseases. Consequently, this can greatly assist dermatologists in precisely identifying the type of disease. Like the technique in [11] [12], deep learning algorithms can also be helpful in the detection of skin cancer.

2. Literature Review

Melanoma is the main cause of death for many people around the world. With the increase in medical and biological data related to skin disease, which greatly helped in analyzing the disease and understanding its conditions, multiple algorithms and machine learning have become the most common and widespread uses in this field [13] [14] [15]. Skin cancer is the most difficult disease. Many researchers have used different types of methodologies dealing with skin cancer, mostly based on skin image data [16][17].

Gómez et al. suggested the Independent Graph Chasing (IHP) method for segmentation of skin lesions. The use of projection images on the first IHP component allows unsupervised lesion segmentation on these images. The segmentation accuracy was satisfactory and could be improved in the future.

The datasets demonstrate the algorithm's robustness and usefulness for dealing with various sorts of illnesses and skin lesions. Using k-means segmentation, the limits were accurately determined [18].

To mitigate the challenge of accurately differentiating between different forms of skin cancer, Singh and Jalal have put out a plan designed to lower the probability of incorrect diagnoses. The method they use involves first removing unnecessary textures from a dataset to improve data organization before grouping it using the K-means algorithm. The pre-processed data is then subjected to feature extraction, improving the outcomes of skin cancer classification. Their approach has a noteworthy 94.4% accuracy rating [19].

A technique designed to help doctors detect skin cancer lesions more precisely has been created by Jaisakthi and colleagues. There are two main steps in their work: First, the pre-processing steps, which include removing hair, marking with a Faringe vessel, and making other picture changes. They also make use of the CLAHE algorithm to improve and standardize lighting. Second, they remove oil from the affected areas using methods like GrabCut and clustering. The lesion is then isolated using clustering and filling techniques, producing edges that are well defined. Both processed and raw data were used to evaluate the procedure, and the test results showed that their goal had been successfully attained [20].

Rahman and his team have addressed the challenge of visually identifying skin damage due to the difficulty in distinguishing between healthy and affected skin. They propose a system based on machine learning and its algorithms, which involves the extraction of specific image data properties. This approach has yielded promising outcomes. In dermatology image assessments, they employ a modified anisotropic filtration technique to distinguish skin spots from noisy images. By using a molten vector and a Hybrid Feature Extractor (HFF) with CNN, they achieved commendable accuracy. The most effective CNN classifier demonstrated excellent accuracy in detecting skin cancer, including non-melanoma skin cancer [21].

Nawaz et al. developed a fully automated method for early-stage cutaneous melanoma segmentation utilizing a deep learning methodology, which is the fastest area-based convolutional neural network (RCNN) in

Doi: https://doi.org/10.54216/FPA.150108
Received: August 12, 2023 Revised: December 10, 2023 Accepted: February 18, 2024

conjunction with the fuzzy k-mean cluster (FKM). The test employs several clinical images. The procedure given here even assists a dermatologist in diagnosing this potentially fatal illness. The sickness is still in its infancy. The approach offered first processes a file Dataset images to reduce noise and lighting issues and improve the visual image. It is faster to establish a fixed feature vector Length before applying RCNN. FKM was then utilized to segment the melanoma-infected leather segment with varied sizes and borders. The results demonstrated its capability in identifying and segmenting skin lesions [22].

3. Methodology

3.1. Dataset

dataset consists of 400 skin picture was utilized; it was retrieved from the Kaggle online repository (https://www.kaggle.com/datasets/hasnainjaved/melanoma-skin-cancer-dataset-of-10000-images)[23]. This dataset has 200 images displaying benign characteristics and 200 images showing signs of malignancy. Images are in JPG-format with dimensions of 444 pixels in width and 359 pixels in height.

The selection of images for this dataset aimed to encompass a diverse array of skin types, colors, and lesion sizes, thereby capturing the comprehensive spectrum of variations present in skin lesions. The images within the dataset have undergone meticulous labeling and grouping, ensuring accurate identification of each sample as either malignant or benign. Through this labeling process, the dataset has been systematically categorized into distinct groups for malignant and benign images, establishing a clear demarcation between the two classes.

3.2. Data Preprocessing

The dataset was divided into twenty groups, with 10 samples from each group representing both benign and malignant cases. the pictures were changed over from the RGB variety space to the Lab variety space. The picture is divided into three distinct channels during this transformation: a, which refers to the red-green pivot, b, which suggests the blue-yellow hub, and L, which displays glow,

This change methodology depends on the CIE Lab variety model, which should be visible in Figure 1. Notwithstanding gadget explicit qualities, the CIE Lab variety model can outwardly address colors in a predictable way. It is possible to independently analyze color-related data by removing the color channels a and b from the transformed CIE Lab image. Besides, the isolated assortment channels went through change into a united exactness plan. When compared to traditional integer or byte representations, this format option guarantees superior accuracy, making it simpler to perform precise analytical procedures and complex computations.

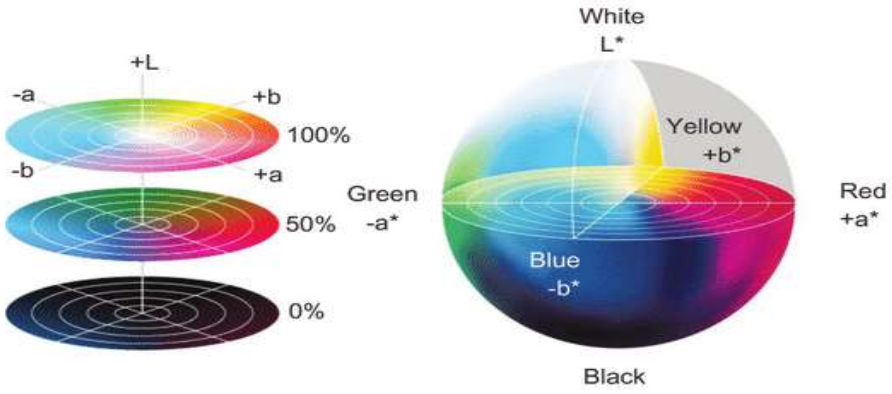

Figure 1: Color characterization is typically accomplished using the CIE Lab color space. There are three parts in this variety space: An address the green-red hub, L denotes delicateness, and B denotes the blue-yellow pivot. A comprehensive description of colors that considers their perceptual properties is possible with this arrangement.

3.3 K-Means Clustering

The K-means clustering algorithm was utilized to categorize the images by examining their color channels a and b, with the goal of dividing skin damage areas based on their color similarities.

K-means clustering is an unsupervised learning technique that groups similar data points together based on their shared features. The predetermined number of clusters determines the level of granularity in color-based segmentation.

Equation 1 represents the algorithm mathematically [25]:

Doi: https://doi.org/10.54216/FPA.150108
Received: August 12, 2023 Revised: December 10, 2023 Accepted: February 18, 2024

$$j = \sum_{i=1}^{N} \sum_{k=1}^{K} w_{ik} \cdot \| x_{i-} c_k \|^2 \quad (1)$$

x_i is a singular data point, $K$is the number of clusters. c represents the set of cluster centroids, c_k represents the centroid of cluster k, $N$is the total number of data points, w_{ik} is a binary indicator (0 or 1) that assigns data point x_i to cluster k . $\| x_{i-} c_k \|^2$ represents the squared Euclidean distance between data point x_i and cluster centroid c_k .

Until convergence is reached, the algorithm iteratively updates the cluster assignments (w_(ik)) and recalculates the cluster centroids (c_(k).

By applying this way to deal with the variety channels an and b, the calculation sections the skin harm district of pictures considering variety closeness, subsequently empowering the extraction of significant variety-based designs inside the dataset.

3.4 Object Segmentation

To perform object segmentation, separate covers were created for each bunch, recognizing pixels related with explicit groups. These masks were binary, with cluster-associated pixels being marked with a value of 1, and non-cluster-associated pixels being marked with a value of 0. The isolated objects that correspond to each cluster were obtained by applying these masks to the original image, making it simpler to carry out subsequent analyses [26]. Equation (2) represents object segmentation mathematically:

$$f_k(x) = \begin{cases} 1, & if\ x\ belongs\ to\ cluster\ k \\ 0, & otherwise \end{cases} \quad (2)$$

$f(x)$ is the binary mask for cluster k. The isolated object I_k for cluster k is obtained by element-wise multiplication of the mask $f_k(x)$with the original image I.

$$I_k(x) = f_k(x) \times I(x) \quad (3)$$

Where x denotes the pixel coordinates.

This process permits the extraction of explicit items or locales of interest relating to each bunch. The resultant disengaged objects I_k can then be exposed to additional investigation, empowering an engaged investigation of unmistakable variety-based designs inside the dataset.

3.5 Luminosity Analysis

The double-dealing of the L (radiance) channel inside the CIE Lab variety space was embraced to intensify the restriction of sores. This required altering the intensity values within the L channel, which improved the contrast and discernibility of the affected areas. The mix of glow examination was utilized to definitively determine the edges of skin sores, subsequently increasing the adequacy of the grouping system.

The change of force values can be addressed as follows [25]:

$$I_{adjusted}(x) = I_{original}(x) \times \alpha \quad (4)$$

Where $I_{original}(x)$is the original intensity values in the L channel. x denotes the pixel coordinates. , $I_{adjusted}$ are the intensity values after adjustment. α as the adjustment factor.

Utilizing this modification in the L channel enhances the contrast and visibility of affected regions, leading to a more precise identification of skin lesions. The enhanced localization which achieved by luminosity analysis, improves the accuracy of classification, and increases the precision of the dataset analysis.

3.6 Histograms Distribution Analysis

The assessment of histograms for the three channels, red (RCC), green (GCC) and blue (BCC) can be enveloped by the investigation of color distribution within each segmented object. Histograms are very important tools in finding out the variation recurrent scattering in the image or within parts of interest. The histograms h_{RCC}, h_{GCC}, and h_{BCC}can be formulated as follows:

$$h_{RCC}(r) = \sum_{x \in I_{obj}} \delta(r - RCC(x)) \quad (5)$$

$$h_{GCC}(g) = \sum_{x \in I_{obj}} \delta(g - GCC(x)) \quad (6)$$

Doi: https://doi.org/10.54216/FPA.150108
Received: August 12, 2023 Revised: December 10, 2023 Accepted: February 18, 2024

$$h_{BCC}(b) = \sum_{x \in I_{obj}} \delta(b - BCC(x)) \quad (7)$$

Where, h_RCC, h_GCC, and h_BCC are the histograms for red, green, and blue channels independently. The disconnected item viable is represented by (I obj). while x indicates the pixel organizes inside the confined article I_obj. RCC(x), GCC(x) and BCC(x) address the red, green, and blue channel variety upsides of pixel x individually. is the Delta function of Dirac [27]. The analysis catches the distribution of color intensities by developing histograms for each channel, offering bits of knowledge into the commonness of explicit tints and shades inside the assigned areas. This quantitative depiction works on the significance of examination performed on the dataset by simplifying it to extricate critical information about assortment features and their assortments inside the divided articles.

3.7 Diagnostic and Classification Range

By calculating the average values of h_RCC, h_GCC, and h_BCC, the precise diagnostic and classification thresholds were determined. The mean values have provided a structure able to accurately diagnose and classify both cancerous and benign lesions. To lay out the classification range, it was essential to identify observable differences in the average color values between the benign and malignant sample groups.

The classification range represents the essential component of this system, this range provides dermatologist with a dependable instrument for exact lesion diagnosis and classification. The typical variety portrayal inside each not set in stone by including all the pixel esteems and isolating by the absolute number of pixels in the group to decide the mean qualities for RCC, GCC, and BCC [28]. The mean (μ) can be calculated mathematically using equation 8:

$$\mu = \frac{\sum x}{n} \quad (8)$$

$\sum x$ represents summation of all pixel values in the cluster, and n is the total number of pixels in the cluster.

For each scenario, 20 sets of benign and malignant patients were taken into consideration when calculating averages. Since each gathering included ten skin tests, it was feasible to assess normal qualities inside the given setting completely. This comprehensive methodology supports more informed medical decision-making by helping to precisely define diagnostic criteria and enhance skin lesion categorization accuracy. This research is a significant focus within the field of healthcare improvement. [29] [30] [31][32][33].

4. Results

In dermatology, examining images of skin lesions is necessary for making an accurate diagnosis and classifying of benign and malignant lesions in dermatology. Our picture examination approach, which luminosity analysis and color-based segmentation, is introduced in this work. The objective is to look further into the variety elements of both solid and harmed skin sores and to recognize the best scale for distinguishing and separating among harmless and threatening examples.

The examination of histogram variety ranges in the first picture, division picture, and glow picture gives significant data to foreseeing whether an example has a place with the harmless or dangerous classification. By contrasting the reaches across these three pieces of the examination, we can decide the most solid scale for precisely distinguishing and grouping harmless and threatening examples as shows in figure 2 and figure 3. The results of our analysis reveal important information regarding the mean color values of the different color channels at various stages of the analysis for both the healthy (benign) and injured (malignant) skin samples.

Doi: https://doi.org/10.54216/FPA.150108
Received: August 12, 2023 Revised: December 10, 2023 Accepted: February 18, 2024

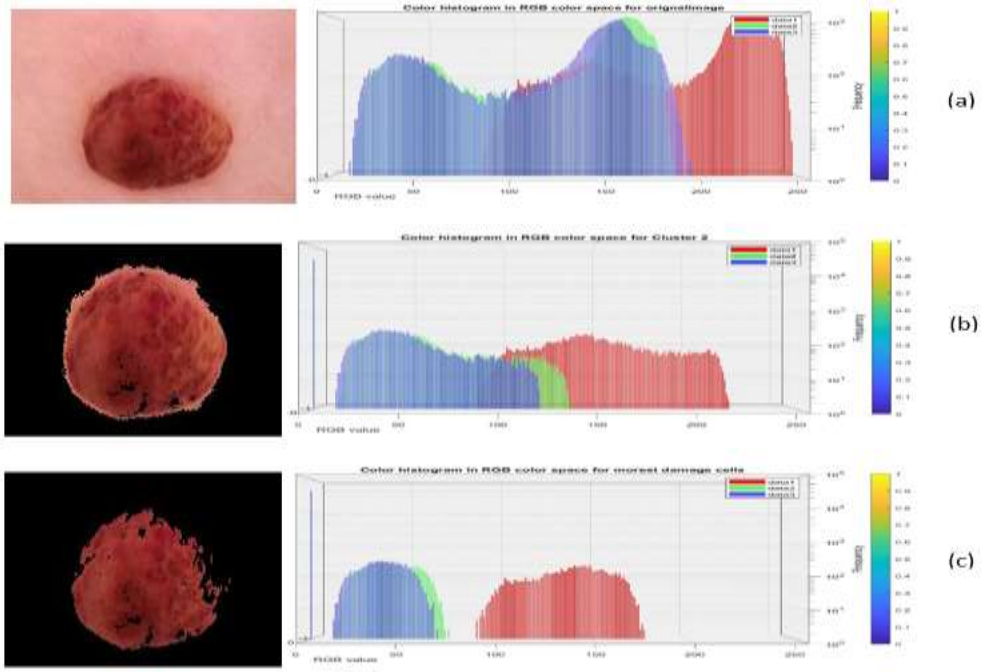

Figure 2: The disparity histograms distribution analysis is observed in the context of a diagnosed benign sample. This assessment encompasses: a) the initial sample, subjected to chromatography analysis; b) the sample post-segmentation, accompanied by its corresponding chromatography analysis; and c) the sample after the restriction of the affected region and the implementation of luminosity analysis.

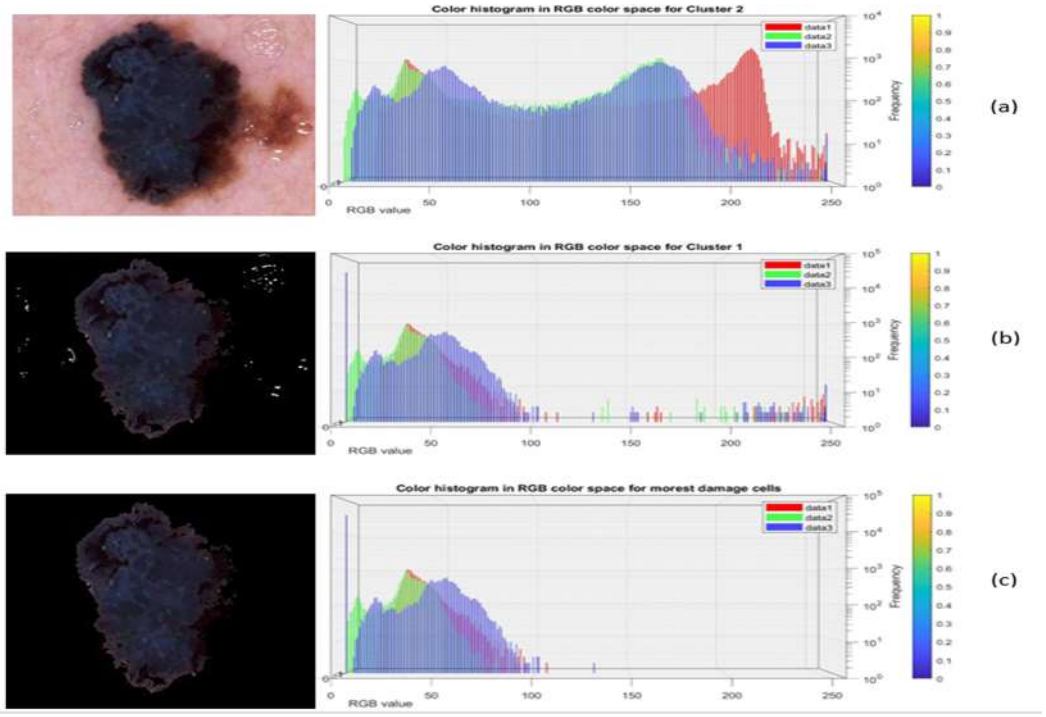

Figure 3: The variation in gradient within the histogram's distribution analysis is examined within the context of a sample diagnosed as malignant. This investigation encompasses: a) the original sample, analyzed through chromatography; b) the sample post-segmentation, along with its corresponding chromatography analysis; and c) the sample after delineating the affected region and implementing luminosity analysis.

Doi: https://doi.org/10.54216/FPA.150108
Received: August 12, 2023 Revised: December 10, 2023 Accepted: February 18, 2024

Table 1: presents the statistical computations for the groups of benign samples across color channels in three distinct scenarios: the original image, the segmented image, and the image following luminosity analysis.

Benign Sample	Original Image			Segmentation Image			Luminosity Image Analysis		
	Mean-RCC	Mean-GCC	Mean-BCC	Mean-RCC	Mean-GCC	Mean-BCC	Mean-RCC	Mean-GCC	Mean-BCC
1st Grope	207.804	175.1929	178.0104	6.6179	4.2404	3.8370	2.2433	0.2638	0.8911
2nd Grope	204.705	192.345	200.642	11.019	5.5814	4.8364	2.4409	0.8540	0.1522
3rd Grope	181.889	153.976	161.371	4.2795	2.8949	2.4949	0.9288	0.5085	0.3049
4th Grope	188.578	155.179	171.6339	4.9946	3.0765	2.5939	1.0597	0.9689	0.7555
5th Grope	185.7835	151.2467	160.3207	8.5142	5.4892	5.3398	2.7160	1.1845	0.0627
6th Grope	196.867	167.751	172.125	10.5867	4.8401	2.4603	2.1321	1.0539	0.780
7th Grope	197.9433	171.9437	198.783	7.8976	5.6107	3.4284	0.969	0.5205	0.4012
8th Grope	193.280	160.124	164.6379	1.3176	0.8331	1.5907	0.2822	0.1336	0.0700
9th Grope	186.648	172.680	183.030	10.815	1.767	2.200	2.259	1.258	0.244
10th Grope	190.336	165.415	175.791	4.289	2.722	2.1294	1.909	1.556	0.7726
11th Grope	189.593	175.5076	177.772	2.381	1.548	1.540	1.1040	0.646	0.5308
12th Grope	201.72	167.987	171.728	4.0284	2.1558	1.879	1.773	0.799	0.9212
13th Grope	239.505	157.020	188.594	10.2496	4.7248	5.5765	2.135	0.551	0.9141
14th Grope	184.642	158.949	176.336	8.4846	4.1781	2.2286	2.7331	1.8601	0.5280
15th Grope	193.4	161.717	185.8737	1.6266	0.869	0.62	0.388	0.1600	0.115
16th Grope	183.735	145.27	186.51	10.3524	5.2008	3.6283	2.2043	0.677	0.952
17th Grope	197.26	182.43	193.056	5.6474	2.555	1.7495	1.5626	1.0055	0.6027
18th Grope	191.19	156.50	175.61	8.7778	4.998	4.1439	2.2782	0.628	0.6605
19th Grope	219.555	176.67	196.67	5.786	4.3627	1.430	1.7964	1.9828	0.1386
20th Grope	194.8524	148.446	188.38	3.2055	2.1567	2.282	1.128	0.6350	0.6369
Range	181.889 239.505	145.27 182.43	171.6339 200.642	2.381 11.019	0.8331 5.6107	1.540 4.8364	0.2822 2.7331	0.1336 1.9828	0.0627 0.9141

Table 2: show grope the statistical analyses conducted on the groups of malignant samples across color channels under three distinct conditions: the original image, the segmented image, and the image subsequent to luminosity analysis

Malignant Sample	Original image			Segmentation image			Luminosity Analysis		
	Mean-RCC	Mean-GCC	Mean-BCC	Mean-RCC	Mean-GCC	Mean-BCC	Mean-RCC	Mean-GCC	Mean-BCC
1st Grope	147.3715	109.4604	113.8500	11.9296	9.6559	4.6248	3.4553	9.1376	1.0706
2nd Grope	148.2398	124.1289	101.8279	13.2185	8.4556	4.7259	3.7900	1.1366	1.1341
3rd Grope	131.2835	109.843	100.9322	17.8347	7.9240	5.7983	3.2458	14.1788	1.1838
4th Grope	159.1862	144.949	132.7122	11.5477	10.0671	4.6509	3.8692	1.0348	0.8610
5th Grope	144.6915	142.577	144.2191	12.0877	8.8452	5.5003	4.6845	1.6175	0.9173
6th Grope	165.7032	135.2881	134.3952	12.0171	8.2762	6.8169	4.6040	2.2953	1.0568
7th Grope	176.8625	148.6367	150.3897	21.2546	9.8040	5.5971	3.9075	2.1930	1.1371
8th Grope	161.3163	84.289	61.5752	11.7969	7.5053	4.9474	3.4552	2.7473	0.9467
9th Grope	155.6142	98.3791	79.833	30.3793	7.0653	4.8882	4.3742	1.1540	0.9111
10th Grope	134.757	92.9109	63.7527	23.8894	7.6495	5.4196	3.7665	1.0529	0.8977
11th Grope	153.666	114.272	120.5985	29.0585	7.3660	5.2576	3.8814	1.4644	1.1727
12th Grope	165.845	142.5740	165.8489	16.6053	8.5113	5.5220	4.6263	1.2081	1.2250
13th Grope	190.153	152.0897	172.7498	11.7541	7.8723	6.3593	3.6908	1.0673	0.8667
14th Grope	179.7481	147.8983	171.6060	11.5879	9.9997	4.6247	3.1461	1.5299	1.3028
15th Grope	188.3947	134.6125	163.6268	12.8528	10.0805	5.5588	4.6281	0.7387	0.8873
16th Grope	180.0629	145.1845	171.3518	24.5761	7.274	5.1823	4.9124	1.4533	1.4543
17th Grope	185.5923	132.886	173.5442	12.8411	7.4660	4.7189	3.4349	1.8951	1.1247
18th Grope	183.8535	148.7124	172.3531	18.8455	9.9296	6.2860	3.0858	2.4897	0.9163
19th Grope	183.3482	143.5892	171.6383	14.2754	8.5096	6.6777	3.3885	0.9806	0.908
20th Grope	170.1264	137.6999	150.1007	15.8517	9.9767	5.6464	3.6079	1.5824	0.8619
Range	131.2835 190.153	84.289 148.7124	61.5752 173.5442	11.5879 30.3793	7.3660 10.0671	4.6247 6.8169	3.1461 4.9124	0.7387 2.7473	0.861 1.5858

Doi: https://doi.org/10.54216/FPA.150108
Received: August 12, 2023 Revised: December 10, 2023 Accepted: February 18, 2024

For the benign samples show in Table 1, in the original image, the highest mean color values are observed in the RCC channel, ranging from 181.889 to 239.505. This indicates a relatively wide range of color values, suggesting the presence of diverse colors or variations in the appearance of benign lesions. On the other hand, the GCC channel exhibits the lowest mean color values, ranging from 145.27 to 182.43. This suggests a narrower range of color values, possibly indicating a more consistent color distribution within the benign lesions as show in Table 2. After applying color-based segmentation, the mean color values in the segmentation image show a significant reduction compared to the original image. The RCC channel has the greatest mean color values, which range from 2.381 to 11.019, while the GCC channel has the lowest mean color values, which range from 0.8331 to 5.6107. This reduction in mean color values can be attributed to the grouping of similar pixels together during segmentation, resulting in a more concentrated color distribution within the segmented regions of the benign lesions. During the luminosity image analysis, the average color values keep getting lower. The goal of this investigation is to improve lesion localization by varying the CIE Lab color space's L channel's intensity values. The GCC channel has the lowest mean color values, ranging from 0.1336 to 1.9828, while the RCC channel has the greatest mean color values, ranging from 0.2822 to 2.7331. The reduction in average color values indicates how well the luminosity analysis performed in enhancing contrast and visibility, which helps the benign areas stand out more. The malignant samples show comparable patterns. The RCC channel in the original image, which ranged from 131.2835 to 190.153, had the highest mean color values. This suggests that the malignant lesions have a variety of color compositions. The GCC channel exhibits the lowest average color values, suggesting a relatively limited color value range of 84.289 to 148. 7124. After segmentation, image exhibits a notable decline in mean color values. With mean color values ranging from 7.3660 to 10.9671, the GCC channel has the lowest mean color values, while the RCC channel has the highest mean color values, from 11.5879 to 30.3793. An increased concentration of color within the divided areas of the malignant lesions is indicated by this decrease in mean color values. During luminosity analysis, the mean color values continue to decrease, with the highest values ranging from 3.1461 to 4.9324 in the RCC channel and the lowest values ranging from 0.7387 to 2.7473 in the GCC channel. This further emphasizes the enhanced visibility and contrast of the malignant areas, facilitating their identification. Classification Range: To establish a range for distinguishing between benign and malignant skin lesions based on the mean color values, a comprehensive analysis of a larger dataset is required. However, the observed ranges can serve as initial reference points. For example, based on the current results, a range of RCC channel mean color values between 181.889 and 239.505 "paraphrasing and highlighted on histogram analyzed for each color channel for each group (consisting of 10 samples after taking the average for them) and the resulting percentages were adopted to diagnose the condition.

Based on these findings, it is evident that the histogram color ranges become narrower and more concentrated as we progress from the original image to the segmentation image and finally to the luminosity image analysis. This indicates that the luminosity analysis provides the most distinct and reliable scale for detecting and classifying benign and malignant samples. The reduced color ranges in the luminosity analysis enhance the contrast and visibility of the lesions, enabling better differentiation between benign and malignant areas.

5. Conclusion

In conclusion, our study offers a novel and reliable approach for correctly classifying benign and malignant skin lesions in dermatology. We have illustrated the possibility of the CIE Lab Color features as a dependable scale for differentiating between these two categories by integrating color-based segmentation with luminosity analysis. With equal representation of benign and malignant samples, we thoroughly evaluated a dataset of 400 skin images to develop a categorization range for accurate diagnosis. We were able to get greater lesion differentiation by using mean color values for the Red Channel Color (RCC), Green Channel Color (GCC), and Blue Channel Color (BCC) in groups of ten samples. To improve contrast and clarity in the photos, our luminosity analysis has identified narrower and more focused color ranges. To further advance the discipline of dermatology, we have highlighted the importance of mean histograms for every color channel.

References

[1] T. Saba, “Computer vision for microscopic skin cancer diagnosis using handcrafted and non-handcrafted features,” Microscopy Research and Technique, vol. 84, no. 6, pp. 1272–1283, 2021, doi: 10.1002/jemt.23686.

[2] L. Ferrante di Ruffano et al., “Optical coherence tomography for diagnosing skin cancer in adults,” Cochrane Database of Systematic Reviews, vol. 2018, no. 12, 2018, doi: 10.1002/14651858.CD013189.

[3] M. Krishna Monika, N. Arun Vignesh, C. Usha Kumari, M. N. V. S. S. Kumar, and E. Laxmi Lydia, “Skin cancer detection and classification using machine learning,” Materials Today: Proceedings, vol. 33, no. August, pp. 4266–4270, 2020, doi: 10.1016/j.matpr.2020.07.366.

Doi: https://doi.org/10.54216/FPA.150108
Received: August 12, 2023 Revised: December 10, 2023 Accepted: February 18, 2024

[4] H. R. Mhaske and D. A. Phalke, "Melanoma skin cancer detection and classification based on supervised and unsupervised learning," 2013 International Conference on Circuits, Controls and Communications, CCUBE 2013, pp. 1–5, 2013, doi: 10.1109/CCUBE.2013.6718539.
[5] V. Madan, J. T. Lear, and R. M. Szeimies, "Non-melanoma skin cancer," The Lancet, vol. 375, no. 9715, pp. 673–685, 2010, doi: 10.1016/S0140-6736(09)61196-X.
[6] J. Cadet and T. Douki, "Formation of UV-induced DNA damage contributing to skin cancer development," Photochemical and Photobiological Sciences, vol. 17, no. 12, pp. 1816–1841, 2018, doi: 10.1039/c7pp00395a.
[7] S. Franceschi, F. Levi, L. Randimbison, and C. La Vecchia, "Site distribution of different types of skin cancer: New aetiological clues," International Journal of Cancer, vol. 67, no. 1, pp. 24–28, 1996, doi: 10.1002/(SICI)1097-0215(19960703)67:1<24::AID-IJC6>3.0.CO;2-1.
[8] "Ultraviolet radiation." https://www.who.int/news-room/fact-sheets/detail/ultraviolet-radiation (accessed Dec. 13, 2022).
[9] R. L. Siegel, K. D. Miller, and A. Jemal, "Cancer statistics, 2015," CA: A Cancer Journal for Clinicians, vol. 65, no. 1, pp. 5–29, 2015, doi: 10.3322/caac.21254.
[10] "Overview -Skin cancer (non-melanoma)." https://www.nhs.uk/conditions/non-melanoma-skin-cancer/.
[11] A. S. I. Al-Obaidi, R. R. O. Al-Nima, and T. Han, "Interpreting Arabic Sign Alphabet by Using the Deep Learning," BIROn - Birkbeck Institutional Research Online BIROn - Birkbeck Institutional Research Online, vol. 23, pp. 71–84, 2022.
[12] A. S. I. Al-Obaidi, R. R. O. Al-Nima, and T. Han, "Interpreting Arabic sign alphabet by utilizing a glove with sensors," International journal of health sciences. pp. 7170–7184, 2022, doi: 10.53730/ijhs.v6ns6.12018.
[13] H. Dashti et al., "Integrative analysis of mutated genes and mutational processes reveals novel mutational biomarkers in colorectal cancer," BMC Bioinformatics, vol. 23, no. 1, 2022, doi: 10.1186/s12859-022-04652-8.
[14] R. Javanmard, K. JeddiSaravi, and H. Alinejad-Rokny, "Proposed a new method for rules extraction using artificial neural network and artificial immune system in cancer diagnosis," Journal of Bionanoscience, vol. 7, no. 6, pp. 665–672, 2013, doi: 10.1166/jbns.2013.1160.
[15] M. R. Mahmoudi, H. Akbarzadeh, H. Parvin, S. Nejatian, V. Rezaie, and H. Alinejad-Rokny, "Consensus function based on cluster-wise two level clustering," Artificial Intelligence Review, vol. 54, no. 1, pp. 639–665, 2021, doi: 10.1007/s10462-020-09862-1.
[16] M. Ahmadinia et al., "Energy-efficient and multi-stage clustering algorithm in wireless sensor networks usin ... Page 1 of 5 Energy-efficient and multi-stage clustering algorithm in wireless sensor networks usin ... Page 2 of 5," pp. 3–8, 2014.
[17] H. Niu, W. Xu, H. Akbarzadeh, H. Parvin, A. Beheshti, and H. Alinejad-Rokny, "Deep feature learnt by conventional deep neural network," Computers and Electrical Engineering, vol. 84, 2020, doi: 10.1016/j.compeleceng.2020.106656.
[18] M. G. T. and J. F. S. Wager and S. RBenjamin, "Independent Histogram Pursuit for Segmentation of Skin Lesions David," Bone, vol. 23, no. 1, pp. 1–7, 2011, doi: 10.1109/TBME.2007.910651.Independent.
[19] S. K. Singh and A. S. Jalal, "A robust approach for automatic skin cancer disease classification," India International Conference on Information Processing, IICIP 2016 - Proceedings, no. Xlm, 2017, doi: 10.1109/IICIP.2016.7975301.
[20] S. M. Jaisakthi, P. Mirunalini, and C. Aravindan, "Automated skin lesion segmentation of dermoscopic images using GrabCut and kmeans algorithms," IET Computer Vision, vol. 12, no. 8, pp. 1088–1095, 2018, doi: 10.1049/iet-cvi.2018.5289.
[21] M. Rahman, M. K. Nasir, and S. I. Khan, "Hybrid Feature Fusion and Machine Learning Approaches for Melanoma Skin Cancer Detection," no. January, 2022, doi: 10.20944/preprints2.
[22] M. Nawaz et al., "Skin cancer detection from dermoscopic images using deep learning and fuzzy k-means clustering," Microscopy Research and Technique, vol. 85, no. 1, pp. 339–351, 2022, doi: 10.1002/jemt.23908.
[23] Hasnain Javed, "Melanoma Skin Cancer Dataset of 10000 Images, " Kaggle, Available: https://www.kaggle.com/datasets/hasnainjaved/melanoma-skin-cancer-dataset-of-10000-images.
[24] A. Gijsenij, T. Gevers, and J. van de Weijer, "Comparison of color spaces for skin lesion segmentation," Skin Research and Technology, vol. 20, no. 4, pp. 444-450, Nov. 2014. doi: 10.1111/srt.12142.
[25] W. R. Fathel, A. S. I. Al-Obaidi, M. A. Qasim, and M. M. Al-Hatab, "Skin Cancer Detection Using K-Means Clustering-Based Color Segmentation," Texas Journal of Engineering and Technology, vol. 18, pp. 46-52, 2023.
[26] T.-Y. Lin, P. Dollár, R. B. Girshick, K. He, B. Hariharan, and S. J. Belongie, "Feature Pyramid Networks for Object Detection," IEEE Conference on Computer Vision and Pattern Recognition (CVPR), June 2017, pp. 936-944. doi: 10.1109/CVPR.2017.106.

Doi: https://doi.org/10.54216/FPA.150108
Received: August 12, 2023 Revised: December 10, 2023 Accepted: February 18, 2024

[27] A. Taner, M. T. Mengstu, K. Ç. Selvi, H. Duran, Ö. Kabaş, İ. Gür, N. E. Gheorghiță, "Multiclass Apple Varieties Classification Using Machine Learning with Histogram of Oriented Gradient and Color Moments," Applied Sciences, vol. 13, no. 13, pp. 7682, 2023. doi: 10.3390/app13137682.
[28] S. Roy, K. Bhalla, and R. Patel, "Mathematical analysis of histogram equalization techniques for medical image enhancement: a tutorial from the perspective of data loss," Multimedia Tools and Applications, pp. 1-30, 2023. doi: 10.1007/s11042-023-13639-1.
[29] W. R. Fathel, A. S. I. Al-Obaidi, M. A. Qasim, and M. M. M. Al-Hatab, "Skin Cancer Detection Using K-Means Clustering-Based Color Segmentation," Texas Journal of Engineering and Technology, vol. 18, pp. 46-52, 2023. doi: 10.1109/TJET.2023.
[30] W. R. Fathel, M. M. M. Al-Hatab, and M. A. Qasim, "Classification ECG Signals Based on k-Nearest Neighbors (k-NN) Algorithm," Eurasian Journal of Engineering and Technology, vol. 16, pp. 41-46, 2023. doi: 10.1109/EJET.2023.
[31] M. M. M. Al-Hatab, R.R.O.Al-Nima, M. A. Qasim, "Classifying Healthy and Infected Covid-19 Cases by Employing CT scan Images " Bulletin of Electrical Engineering and Informatics, vol. 11, no. 6, pp. 3279-3287, 2022. doi: 10.11591/eei.v11i6.4344.
[32] E. Y. Abd-jabbar, M. M. M. Al-Hatab, M. A. Qasim, M. A. Fadhil, "Clinical Fusion for Real- Time Complex QRS Pattern Detection in Wearable ECG Using the Pan-Tompkins Algorithm," Fusion: Practice and Application (FPA),vol.12, no. 2, PP.172-184 , 2023,doi: 10.54216/FPA.120214.
[33] R.R.O.Al-Nima, M. M. M. Al-Hatab, M. A. Qasim, "An Artificial Intelligence Approach for Verifying Persons by Employing the Deoxyribonucleic Acid (DNA) Nucleotides" Journal of Electrical and Computer Engineering, Vol 2023 , doi:10.1155/2023/6678837.

Doi: https://doi.org/10.54216/FPA.150108
Received: August 12, 2023 Revised: December 10, 2023 Accepted: February 18, 2024